Numerical Simulations on the Perforation of Metal Plates under Normal Impact by Conical-nosed Projectiles

Wu Qiaoguo[1,*], **Wen Heming**[2]

[1] National Technology Research Center on Pressure Vessel and Pipe Line Safety Engineering, Hefei General Machinery Research Institute, Hefei 230031, China
[2] CAS Key Laboratory for Mechanical Behavior and Design of Materials, University of Science and Technology of China, Hefei 230027, China
* Corresponding author: wuqiaoguo1015@163.com

Abstract This paper examines the perforation of Weldox460E steel plates struck normally by rigid conical-nosed projectiles through numerical simulations. The modified Johnson-Cook constitutive relation and the Gruneisen equation of state for metal plates are implemented in ABAQUS/Explicit as a user-defined material model by means of a subroutine (VUMAT). Numerical simulations are conducted on the perforation of Weldox460E steel plates struck normally by conical-nosed projectiles and flat-ended projectiles, it is shown that the numerical results are in good agreement with experiments. Finally, the effects of various cone angles of conical-nosed projectiles on the failure modes of metal plates and the energies absorbed for perforation are discussed.

Keywords Metal plates; Conical-nosed projectiles; Impact; Perforation; Numerical simulation

1. Introduction

An understanding of the response of structures subjected to intense dynamic loads which produce large inelastic deformation and failure is very important for safety calculations and assessment in various engineering such as nuclear, chemical, transport, offshore, naval, aerospace, and defense industries. In particular, the deformation and perforation behavior of plates is important for the design of offshore and protective structures against projectiles, fragments generated from explosion or dropped objects. The problem has been extensively studied in the past, and several studies are available in literature. Comprehensive reviews on the subject can be found in the papers by Backman and Goldsmith [1], Corbett et al. [2], and Goldsmith [3].

Borvik et al. [4-6] carried out experimental and axi-symmetric numerical investigation of Weldox steel plates struck normally by blunt, hemispherical and conical nosed projectiles. The effects of target strength and projectile nose shape on the failure modes and ballistic limits of steel plates are studied. Rosenberg et al. [7] examined the process of ductile plate perforation by sharp-nosed rigid projectiles through 2D numerical simulations, and the normalized resisting stress exerted by the plates can be simply related to the normalized thickness of the plates.

Iqbal et al. [8, 9] performed three-dimensional numerical simulations to study the behavior of ductile targets subjected to normal and oblique impact by sharp nosed cylindrical projectiles. Gupta et al. [10] dealed with the experimental and numerical investigations of aluminum target plates impacted by blunt, ogive and hemispherical nosed steel projectiles, and the effect of projectile nose shape, impact velocity and plate thickness on the deformation of the target plates was studied. Sun [11] carried out axi-symmetric numerical simulations of Weldox460E steel plates struck normally by flat-ended and conical-nosed projectiles using a viscoplastic constitutive model combined with ductile damage.

In this paper, numerical simulations are conducted on the perforation of Weldox460E steel plates struck normally by rigid conical-nosed projectiles and flat-ended projectiles. The modified Johnson-Cook constitutive relation and the Gruneisen equation of state which are valid for metals subjected to impact for large strains, high strain rates and high temperatures are implemented in ABAQUS/Explicit as a user-defined material model by means of a subroutine (VUMAT). Comparisons of the numerical results and the experiments show that the finite element models developed here are reliable. Based on the verified finite element model, numerical simulations are performed on the perforation of 6mm thick Weldox460E steel plates struck normally by conical-nosed projectiles with various cone angles, and the effects of various cone angles on the failure modes of metal plates and the energies absorbed for perforation are discussed.

2. Numerical simulation

In this section, numerical simulations are conducted on the perforation of Weldox460E steel plates struck normally by rigid conical-nosed projectiles and flat-ended projectiles, the cone angles of which are equal to 180^{o} as a special case of conical-nosed projectiles, using dynamic finite element code ABAQUS/Explicit. The targets was modelled using the modified Johnson-Cook constitutive relation which was implemented as a user-defined material model by means of a subroutine (VUMAT).

2.1. Finite element model

Finite element model in this section is based on the experiments of normal impact of Weldox460E steel plates by conical-nosed projectiles and flat-ended projectiles [4][12]. The projectiles have a nominal mass (G) and diameter ($d=2a$) of 197g and 20mm, respectively. The total length (L) and the cone angle (θ) of the conical-nosed projectile is 98mm and 33^{o}, and the total length (L) of the flat-ended projectile is 80mm. Projectiles were manufactured from Arne tool steel which has high strength and hardness, and it was observed that the plastic deformation of the projectiles was very small after perforation. In order to save CPU time and raise computational efficiency, projectiles are assumed to be rigid here. The target plates, having a span diameter ($S=2R$) of 500mm, were restrained at their periphery with respect to all degree of freedoms. Quarter models are used in the 3D finite element analysis, as seen in Fig. 1.

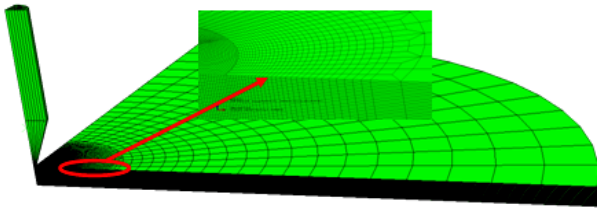

(a) Conical-nosed projectile

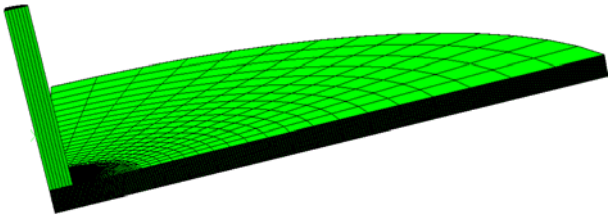

(b) Flat-ended projectile

Figure 1. Finite element model for Weldox460E steel plate struck normally by conical-nosed and flat-ended projectile.

As shown in Fig.1, the target was meshed with eight node brick elements, and all the meshes contained three regions: a finely zoned region which had noticeable effect on computational accuracy, a coarsely zoned region which did not have noticeable effect on computational accuracy, and a transitional region between the two regions above. The meshing method adopted here resolved the contradiction between mesh size and computational accuracy and efficiency to some extent. The element size in finely zoned region was taken to be 0.3mm×0.3mm×0.3mm approximately [5][9]. The diameter of the finely zoned region was 18mm (about 1.5 times as great as projectile diameter). The element size in transitional region and coarsely zoned region was increased from the central part to the outer part of the target. The element type used in the model was 8-node reduced integration elements (C3D8R). Contact between the projectile and target was assigned using the general contact algorithm. The value of coefficient of friction was hard to be measured accurately from experiments, and often taken to be 0~0.05 in literatures for penetration and perforation of metal plates by conical-nosed projectiles [5][7][11][13], and a coefficient of friction of 0.03 was considered here. For the perforation of Weldox460E steel plates by flat-end projectiles, a coefficient of friction of 0.0 was considered [10-12].

2.2. Constitutive relation

The modified Johnson-Cook constitutive relation is adopted for Weldox460E steel target [6]. The model includes linear thermoelasticity, the von Mises yield criterion, the associated flow rule, isotropic strain hardening, strain-rate hardening and softening due to adiabatic heating, and is valid for metals subjected to large strains, high strain rates and high temperatures. The equivalent stress is expressed as

$$\sigma_{eq} = \left(A + B\varepsilon^{n}{}_{eq}\right)\left(1 + \dot{\varepsilon}^{*}_{eq}\right)^{c}\left(1 - T^{*m}\right) \tag{1}$$

where A，B，C，n，m are material constants; ε_{eq} is the equivalent plastic strain; $\dot{\varepsilon}^{*}_{eq} = \dot{\varepsilon}_{eq}/\dot{\varepsilon}_{0}$ is the dimensionless strain rate, where $\dot{\varepsilon}_{0}$ is a user-defined reference strain rate; $T^{*} = \left(T - T_r\right)/\left(T_m - T_r\right)$ is the homologous temperature, where T is the absolute temperature, T_r is the room temperature, T_m is the melting temperature of the target material, respectively.

Johnson and Cook also developed a failure criterion that accounts for temperature, strain rate

and strain path in addition to the triaxiality of the stress state. The damage variable D has the basic form

$$D = \sum \frac{\Delta \varepsilon_{eq}}{\varepsilon_f} \tag{2}$$

where $\Delta\varepsilon_{eq}$ is the increment of accumulated plastic strain and ε_f is the fracture strain given as

$$\varepsilon_f = \left(D_1 + D_2 \exp\left(D_3 \sigma^*\right)\right)\left(1 + \dot{\varepsilon}^*_{eq}\right)^{D_4}\left(1 + D_5 T^*\right) \tag{3}$$

where D_1、D_2、D_3、D_4、D_5 are material constants, $\sigma^*=\sigma_H/\sigma_{eq}$ is the stress triaxiality ratio and σ_H is the mean stress. The temperature increment (ΔT) during perforation is calculated as

$$\Delta T = \int_0^{\varepsilon_{eq}} \chi \frac{\sigma_{eq} d\varepsilon_{eq}}{\rho_t C_p} \tag{4}$$

where ρ_t is the material density, C_p is the specific heat, χ is the coefficient that represents the proportion of plastic work converted into heat.

The damage variable D (Eq. 2) takes values between 0 (undamaged) and 1 (fully broken). When the damage variable D equals to 1, the damaged element will be removed from the mesh in the simulations. Meanwhile, the erosion strain (ε_c) of 2.0 is defined in the simulations in order to ensure that elements which are heavily deformed will not stop the computation process. The erosion strain (ε_c) of 2.0 is high enough to avoid any problems with mass erosion in the target [7]. When the equivalent plastic strain (ε_{eq}) is greater than the erosion strain (ε_c), the element will be removed.

The Gruneisen equation of state is employed, viz.

$$P = \rho_t C_0^2 \frac{\lambda}{(1 - s_1 \lambda)^2}\left(1 - \frac{\Gamma_0 \lambda}{2}\right) + \Gamma_0 \rho_t E_m \tag{5}$$

where P is hydrostatic pressure, C_0, S_1 and Γ_0 are material constants, E_m is specific internal energy of target material, and $\lambda = 1 - V/V_0$, where V is current volume and V_0 is initial volume.

The material parameters for Weldox460E steel target given in Table 1 are taken from Dey et al. [6]. E is the elastic moduli and ν is the Poisson's ratio of the target.

2.3. Simulation results

Fig.2 shows comparisons of the simulation results and the experimental data obtained by Borvik et al. [4] in terms of residual velocity for 12mm thick Weldox460E steel plates struck normally by conical-nosed projectiles with diameter (20mm), mass (197g) and cone angle (θ=33^o). Fig.3 shows comparisons of the simulation plot and the experimental image of the target after full perforation when the strike velocity of the projectile is 300.3m/s.

Table 1. Material parameters for Weldox460E steel targets [6]

E (GPa)	210	D_3	-2.969
ν	0.33	D_4	-0.014
ρ_t (kg/m^3)	7850	D_5	1.014
A (MPa)	499	C_p (J/kgK)	452
B (MPa)	382	χ	0.9
n	0.458	T_m (K)	1800
$\dot{\varepsilon}_0$ (s^{-1})	5×10^{-4}	T_r (K)	293
C	0.0079	C_0 (km/s)	3.574
m	0.893	S_1	1.920
D_1	0.636	Γ_0	1.69
D_2	1.936		

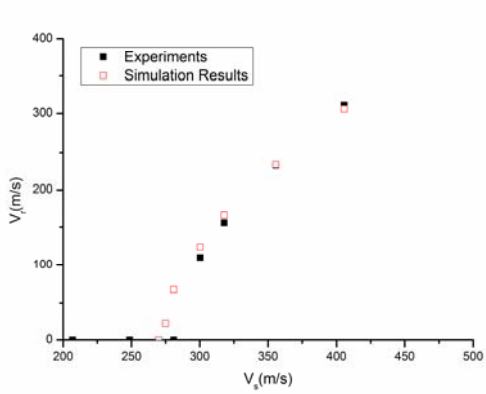

Figure 2. Comparisons of the simulation results with the experimental data [4] in terms of residual velocity for 12mm thick Weldox460E steel plates struck normally by conical-nosed projectiles.

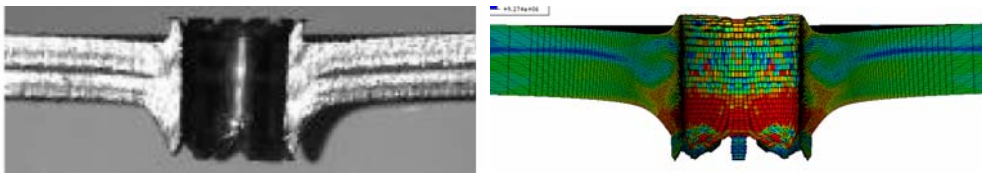

Figure 3. Comparisons of the simulation plot and the experimental image of 12mm thick Weldox460E steel plate after full perforation.

Fig.4 shows comparisons of the simulation results and the experimental data obtained by Borvik et al. [12] in terms of residual velocity for 6mm and 16mm thick Weldox460E steel plates struck normally by flat-ended projectiles with diameter (20mm), mass (197g). Fig.5 shows comparisons of the simulation plot and the experimental image of the plate after full perforation.

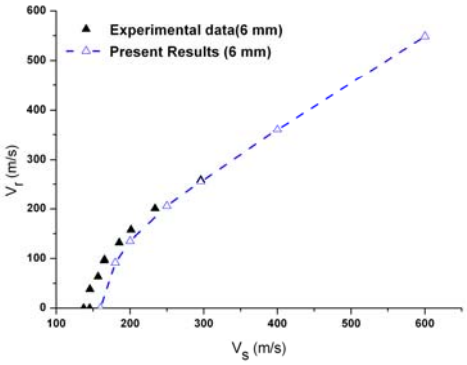

(a) 6mm thick Weldox460E steel plates

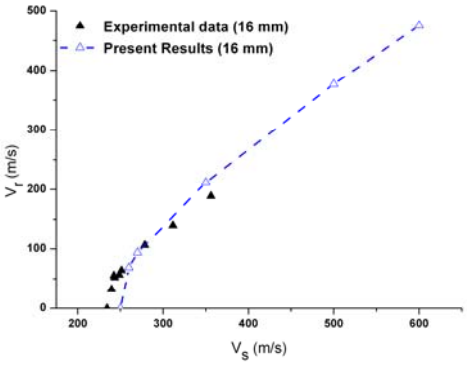

(b) 16mm thick Weldox460E steel plates

Fig.4 Comparisons of the simulation results with the experimental data [12] in terms of residual velocity for 6mm and 16mm thick Weldox460E steel plates struck normally by flat-ended projectiles.

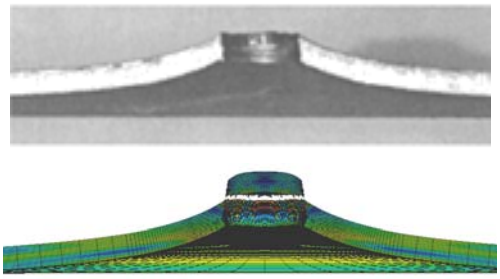

(a) 6mm thick Weldox460E steel plates

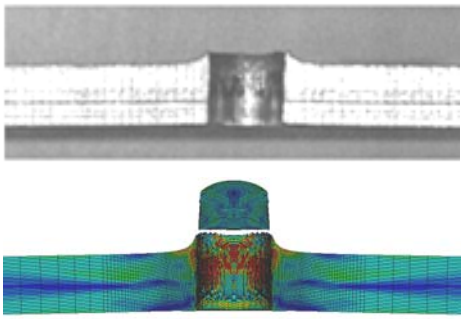

(b) 16mm thick Weldox460E steel plates

Fig.5 Comparisons of the simulation plot and the experimental image of 6mm and 16mm thick Weldox460E steel plate after full perforation.

It is evident from Fig.2 to Fig.5 that the simulation results are in good agreement with the experimental results, and the finite element model is reliable. Based on the present FE model, perforation of 6mm thick Weldox460E steel plates struck normally by rigid conical-nosed projectiles with various cone angles will be analyzed in the following section.

3. Numerical simulations for conical-nosed projectiles with various cone angles

In this section, the perforation behaviors of 6mm thick Weldox460E steel plates under normal impact by conical-nosed projectiles with cone angle θ=20 °、 60°、 100° and 140° are analyzed by numerical simulations. The projectiles with various cone angles have the same effective length L_{eff}, $L_{eff} = 4M/\left(\rho_t \pi d^2\right)$, the diameter ($d$) and the mass ($M$) of which are 20mm and 197g, respectively. Thus, the total lengths of projectiles with θ=20 °、60°、100° and 140° are 111.2mm, 88.9mm, 83.9mm and 81.2mm, respectively. The strike velocities of the projectiles are 200 m/s.

Fig.6 shows the perforation process of 6mm thick Weldox460E steel plate under normal impact by conical-nosed projectile with θ=20° through numerical simulation. It can be seen clearly from Fig.6 that the materials accumulated aside the perforation hole is formed by radial expansion. Thus, it is deduced that the dominant failure mode here is ductile hole enlargement with global deformation.

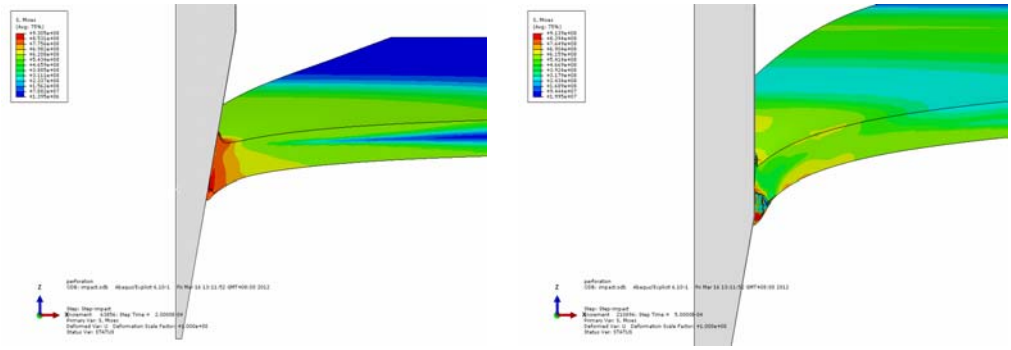

Figure 6. The perforation process of 6mm thick Weldox460E steel plate under normal impact by projectile with θ=20° through numerical simulation.

Fig.7 shows the perforation process of 6mm thick Weldox460E steel plate under normal impact by conical-nosed projectile with θ=60° through numerical simulation. It can be seen clearly from Fig.7 that local bending occurs for the materials beside the projectile, and the dominant failure mode is classified to petalling with global deformation.

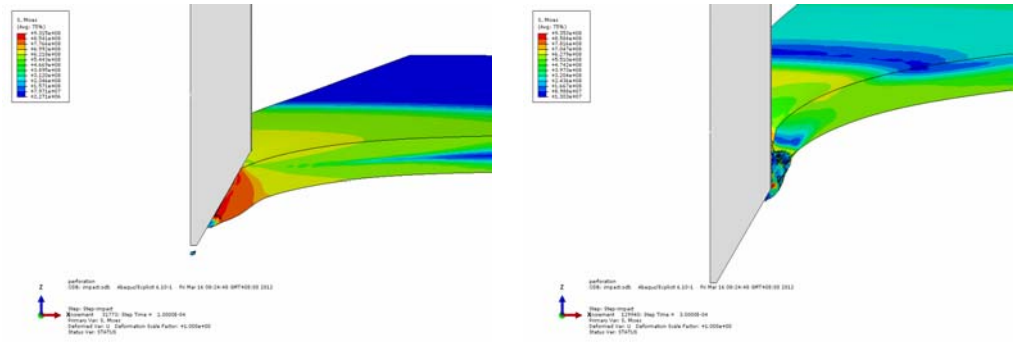

Figure 7. The perforation process of 6mm thick Weldox460E steel plate under normal impact by projectile with θ=60^{o} through numerical simulation.

Fig.8 shows the perforation process of 6mm thick Weldox460E steel plate under normal impact by conical-nosed projectile with θ=100^{o} through numerical simulation. It can be seen from Fig.8 that a plug of diameter larger than the diameter of the projectile is ejected. The crack occurs firstly at the distal surface of the plate, and then propagates to the frontal surface of the plate, finally a full plug is ejected due to stretching and shearing. The plug is formed due to the mixed failure mode of stretching and shearing, and the failure mode here is classified to discing with global deformation.

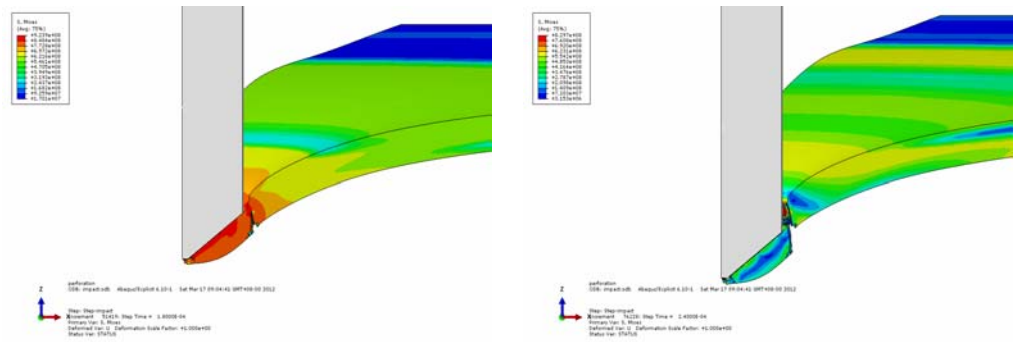

Figure 8. The perforation process of 6mm thick Weldox460E steel plate under normal impact by projectile with θ=100^{o} through numerical simulation.

Fig.9 shows the perforation process of 6mm thick Weldox460E steel plate under normal impact by conical-nosed projectile with θ=140^{o} through numerical simulation. It can be seen from Fig.9 that a plug is ejected which is similar to that in Fig.8, but the difference is that the diameter of the plug here is less than that in Fig.8, which is approximately equal to the diameter of the projectile. The plug is formed mainly due to the failure mode of shearing, and the failure mode here is classified to plugging with global deformation.

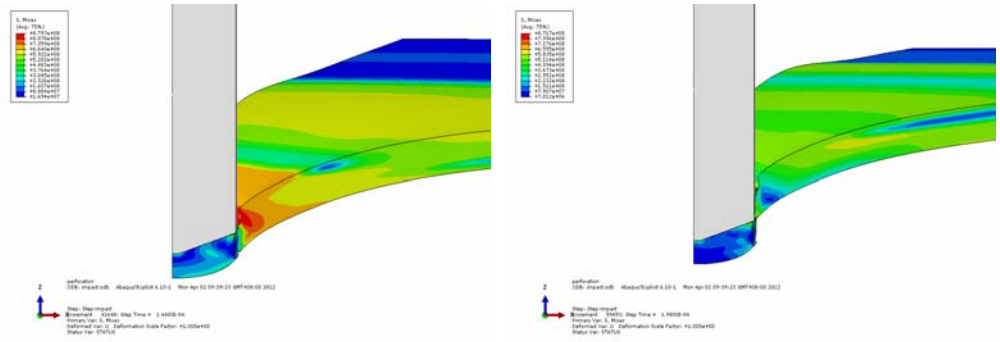

Figure 9. The perforation process of 6mm thick Weldox460E steel plate under normal impact by projectile with θ=140^o through numerical simulation.

As seen from Fig.6 to Fig.9, it is shown that projectile cone angle has significant effect on the perforation modes of 6mm thick Weldox460E steel plates and that for smaller cone angles plates fail by ductile hole enlargement, for medium cone angles plates fail by petalling and for larger cone angles plates fail by discing or plugging.

Fig.10 shows the numerical residual velocity V_r for 6mm thick Weldox460E steel plates struck normally by conical-nosed projectiles with θ=20^o, 60^o, 100^o and 140^o.

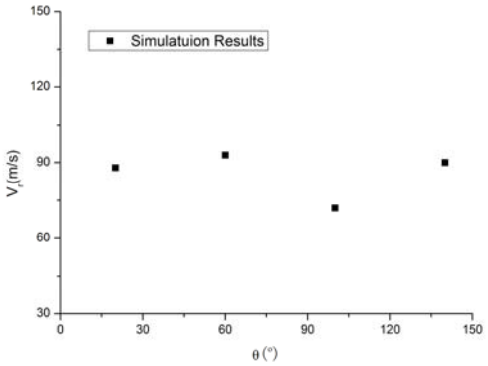

Figure 10. Numerical residual velocity V_r for 6mm thick Weldox460E steel plates struck normally by conical-nosed projectiles with various cone angles

As shown in Fig.10, the residual velocity of projectile is closely related to the failure mode of the target plate, and the residual velocity is not always decreasing sensuously with the increment of the projectile cone angles. The residual velocities for various projectile cone angles θ=20^o, 60^o, 100^o and 140^o in present simulations are 88m/s, 93m/s, 72m/s and 90m/s, respectively. The energy dissipated for the perforation of target plate failed in ductile hole enlargement with global deformation struck normally by conical-nosed projectile with θ=20^o is larger than that for the perforation of target plate failed in petalling with global deformation struck normally by conical-nosed projectile with θ=60^o. The energy dissipated for the perforation of target plate failed in discing with global deformation struck normally by conical-nosed projectile with θ=100^o is larger than those by projectile cone angle θ=20^o and 60^o, and obviously larger than that for the perforation of target plate failed in plugging with global deformation struck normally by conical-nosed projectile with θ=140^o. It is found that the energy dissipated by discing is maximum.

3. Conclusions

In the present paper, a numerical study has been conducted on the perforation of Weldox460E steel plates subjected to impact by rigid conical-nosed projectiles at normal incidence using dynamic finite element code ABAQUS/Explicit. The targets was modelled using the modified Johnson-Cook constitutive relation which was implemented as a user-defined material model by means of a subroutine (VUMAT). The numerical results are in good agreement with the experiments in terms of the patterns of targets after full perforation and the residual velocities, it is shown that the finite element models developed here are reliable. Based on the verified finite element model, numerical simulations are performed on the perforation of 6mm thick Weldox460E steel plates struck normally by conical-nosed projectiles with various cone angles. It is found that the energy dissipated for the perforation is closely related to the failure mode of the target plate, and the energy dissipated is not always increasing sensuously with the increment of the projectile cone angles. It is shown that the energy dissipated by discing is maximum.

References

[1] Backman ME, Goldsmith W. The mechanics of penetration of projectiles into targets. International Journal of Engineering Science, 1978, 16(1): 1-99.

[2] Corbett GG, Reid SR, Johnson W. Impact loading of plates and shells by free-flying projectiles: a review. International Journal of Impact Engineering, 1996, 18(2): 141-230.

[3] Goldsmith W. Non-ideal projectile impact on targets. International Journal of Impact Engineering, 1999, 22(2-3): 95-395.

[4] Borvik T, Langseth M, Hopperstad OS, Malo KA. Perforation of 12 mm thick steel plates by 20 mm diameter projectiles with flat, hemispherical and conical nosed part Ⅰ: experimental study. International Journal of Impact Engineering. 2002, 27(1): 19-35.

[5] Børvik T, Hopperstad OS, Berstad T, Langseth M. Perforation of 12mm thick steel plates by 20mm diameter projectiles with flat, hemispherical and conical noses, Part Ⅱ: numerical simulations. International Journal of Impact Engineering. 2002, 27(1): 37-64.

[6] Dey S, Børvik T, Hopperstad OS, Leinum JR, Langseth M. The effect of target strength on the perforation of steel plates using three different projectile nose shapes. International Journal of Impact Engineering. 2004, 30(8–9): 1005–1038.

[7] Rosenberg Z, Dekel E. Revisiting the perforation of ductile plates by sharp-nosed rigid projectiles. International Journal of Solids and Structures. 2010, 47: 3022-3033.

[8] Iqbal MA, Chakrabarti A, Beniwai S, Gupta NK. 3D numerical simulations of sharp nosed projectile impact on ductile targets. International Journal of Impact Engineering. 2010, 37: 185-195.

[9] Iqbal MA, Gupta G, Gupta NK. 3D numerical simulations of ductile targets subjected to oblique impact by sharp nosed projectiles. International Journal of Solids and Structures. 2010, 47: 224-237.

[10] Gupta NK, Iqbal MA, Sekhon GS. Effect of projectile nose shape, impact velocity and target thickness on deformation behavior of aluminum plates. International Journal of Solids and Structures. 2007, 44: 3411-3439.

[11] Sun WH. Theoretical and numerical study on failure modes of metal plates under normal impact by conical-nosed projectiles. PHD Dissertation, University of Science and Technology of China, 2009.

[12] Børvik T, Hopperstad OS, Langseth M, Malo KA. Effect of target thickness in blunt projectile penetration of Weldox 460 E steel plates. International Journal of Impact Engineering. 2003, 28: 413-464.

[13] He T. A study on the penetration of projectiles into targets made of various materials. PHD Dissertation, University of Science and Technology of China, 2007.